Ionics (2019) 25:81–87
https://doi.org/10.1007/s11581-018-2569-4

ORIGINAL PAPER

Morphology and particle growth of Mn-based carbonate precursor in the presence of ethylene glycol for high-capacity Li-rich cathode materials

Yanhong Xiang[1,2] · Jian Li[1,2] · Qijun Liao[1,2] · Xianwen Wu[2]

Received: 11 March 2018 / Revised: 16 April 2018 / Accepted: 18 April 2018 / Published online: 2 May 2018
© Springer-Verlag GmbH Germany, part of Springer Nature 2018

Abstract

Mn-based carbonate precursor ($Ni_{0.15}Co_{0.15}Mn_{0.7}CO_3$) is synthesized by the carbonate precipitation in the presence of ethylene glycol. The nucleation and growth of precursor particles are investigated during the precipitation process by monitoring particle morphologies and structures. Primarily irregular-shaped and micron-sized loose agglomerate particles are formed and then the particles grow gradually and continue to aggregate with a round shape. After 3.5 h, obvious segregation is observed within the agglomerations. Finally, the particles obtained after aging overnight have a spherical shape and dispersed with a narrow size distribution. The additive of ethylene glycol shows significant effects on the morphology of the prepared $Ni_{0.15}Co_{0.15}Mn_{0.7}CO_3$ and the electrochemical performance of lithiated $Li_{1.2}Ni_{0.12}Co_{0.12}Mn_{0.56}O_2$.

Keywords Mn-based carbonate precursor · Cathode material · Li-rich material · Ethylene glycol · Li-ion battery

Introduction

Lithium-ion batteries (LIBs) have been widely used in mobile electronic devices in recent years and have been regarded as one of promising power source candidates for other fields such as electric vehicles and energy storage power station [1–8]. The demands for the next-generation LIBs have focus on the energy density, safety, and cost. Among the LIB cathode materials ($LiMn_2O_4$, $LiCoO_2$, $LiNiCoMnO_2$, $LiFePO_4$, et al.), lithium manganese oxides have unique advantages such as safe, cheap, and low toxic and, therefore, can be considered the promising cathode material [9, 10]. Recently, Li-rich Mn-based layered compounds ($Li_2MnO_3{\cdot}LiMO_2$ or $Li[M_{1-x}Li_x]O_2$ (M = Mn, Ni, Co, etc.)), which are solid solutions between the monoclinic Li_2MnO_3 (C2/m symmetry) phase and trigonal $LiMO_2$ ($R\bar{3}m$ symmetry) phase, have attracted a significant amount of interest because of their encouraging high reversible capacity (> 200 mAh g^{-1}) when cycled between 2.0~4.8 V [11–14]. Synthesizing technology has a great impact on the micromorphology and structure and subsequently affects the electrochemical performances. The hydroxide co-precipitation method was the usual synthesis method used to produce these materials [15, 16]. However, the metal Mn^{2+} ion can easily be oxidized to Mn^{3+} (MnOOH) or Mn^{4+} (MnO_2) during the hydroxide co-precipitation process, therefore, resulting in inhomogeneous and impure phases in final product [17, 18]. Fortunately, in carbonate precipitation method, the oxidation state of the Mn ions is kept as 2+ in aqueous solution; thereby, it can be used for the synthesis of a more homogeneous and pure Li-rich Mn-based layered material with high electrochemical performance [19].

Co-precipitation of two or more metal ions homogeneous is a challenging process. Besides the polymetallic precipitation reactions, several other co-precipitation conditions such as ligand concentration, pH, stirring rate, and feeding sequence are important to the nucleation and growth of particles and, therefore, to the morphology of the final product [20–23]. However, no comprehensive study is available in the literature on the carbonate particle growth as a function of reaction time. The present research gives insights into the nucleation and

✉ Yanhong Xiang
112301009@csu.edu.cn

[1] School of Physics and Mechanical and Electrical Engineering, Jishou University, Jishou 416000, Hunan, China

[2] The Collaborative Innovation Center of Manganese-Zinc-Vanadium Industrial Technology (the 2011 Plan of Hunan Province), Jishou 416000, Hunan, China

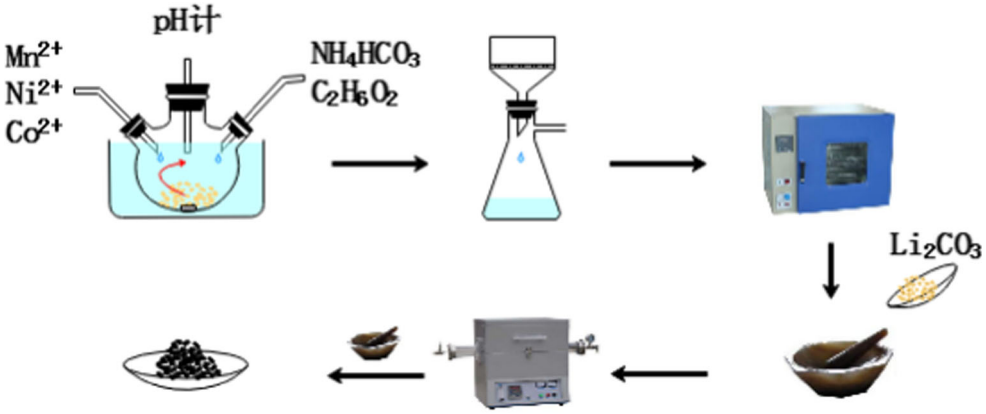

Fig. 1 Schematic illustration on the formation process of sample

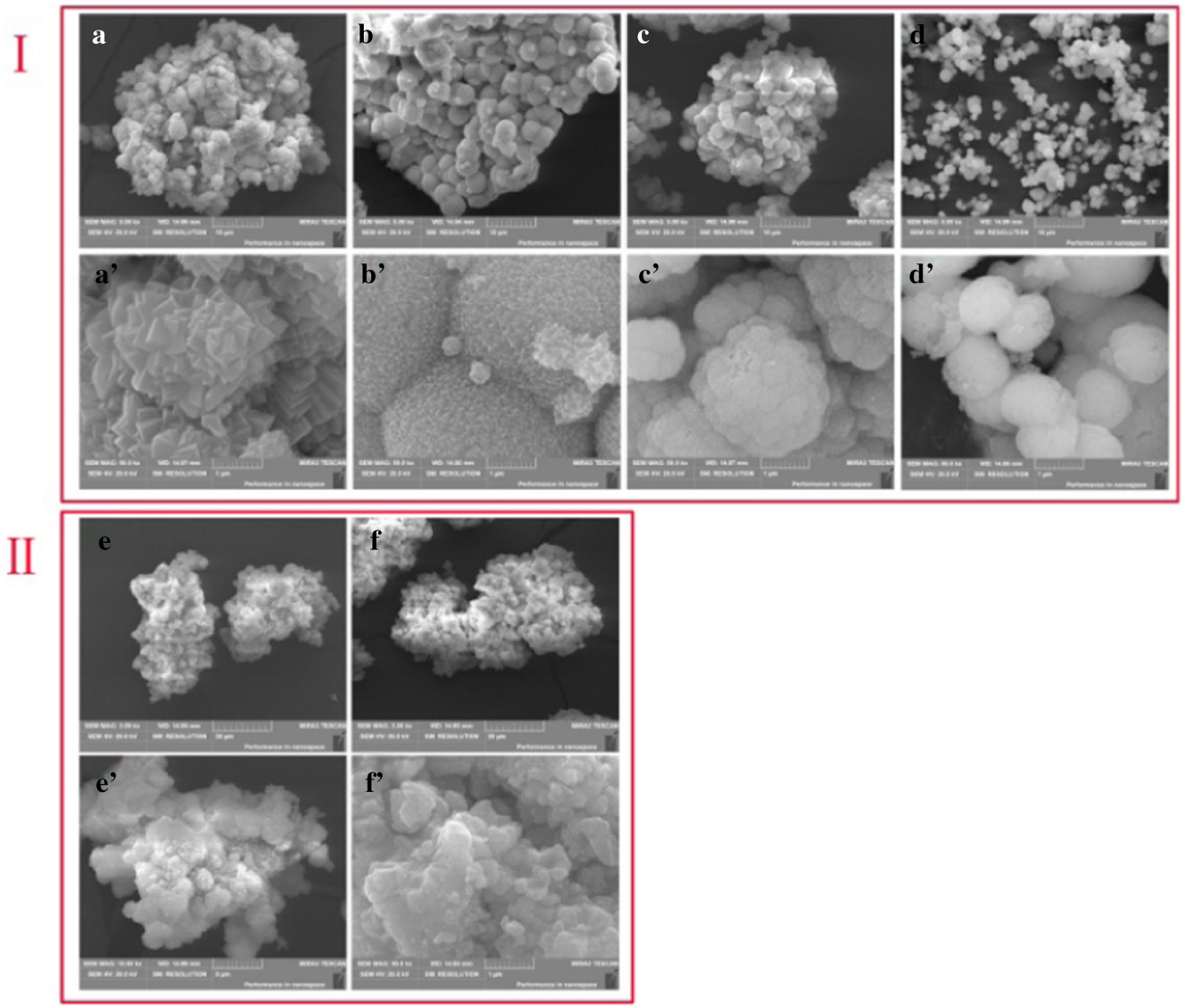

Fig. 2 SEM images of $Ni_{0.15}Co_{0.15}Mn_{0.7}CO_3$ collected at different reaction times. (I) EG-precursors (precursors collected in the presence of ethylene glycol), 2.5 h (a, a'), 3 h (b, b'), 3.5 h (c, c'), aging overnight (d, d'). (II) The pristine (precursors collected without ethylene glycol), 2.5 h (e, e'), aging overnight (f, f')

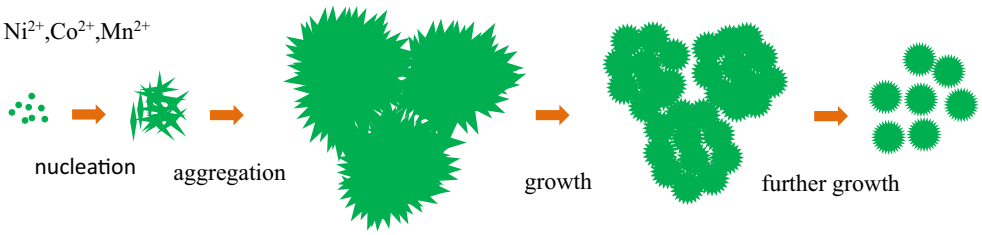

Fig. 3 Schematic illustration for the overall formation process of microspheres of the EG-precursor

growth mechanism of precursors prepared by the carbonate co-precipitation process in the presence of ethylene glycol. We experimentally monitored the nucleation and growth processes by analyzing the particle morphology and structure as a function of the reaction time. The structure, morphology, and electrochemical performance of the final cathode materials are also analyzed.

Experimental

All the reagents used in the present work were of guaranteed grade and used without further purification. Reagents used in this investigation included nickel sulfate hexahydrate ($NiSO_4 \cdot 6H_2O$), manganese sulfate monohydrate ($MnSO_4 \cdot H_2O$), cobalt sulfate heptahydrate ($CoSO_4 \cdot 7H_2O$), and ammonium bicarbonate (NH_4HCO_3), ethylene glycol (EG), and lithium carbonate (Li_2CO_3). The precursors were prepared as follows: an equal volume of 0.15 mol L^{-1} NH_4HCO_3 solution was added into a mixture of 0.15 mol L^{-1} MSO_4 (Ni:Co:Mn 0.15:0.15:0.70) and an appropriate volume of ethylene glycol under vigorous agitation in the temperature of 55 °C. In the process of preparing precursors, the ammonium bicarbonate (NH_4HCO_3) solution serves as not only a reservoir for precipitating anions but also complexing agents. The precipitated powders were filtered and washed and then dried at 105 °C overnight. The obtained precursors were thoroughly mixed with Li_2CO_3 and then calcined at 950 °C for 10 h in air to obtain the final cathode material. The synthesis process is illustrated in Fig. 1. The pristine sample (without ethylene glycol) was also prepared for comparison.

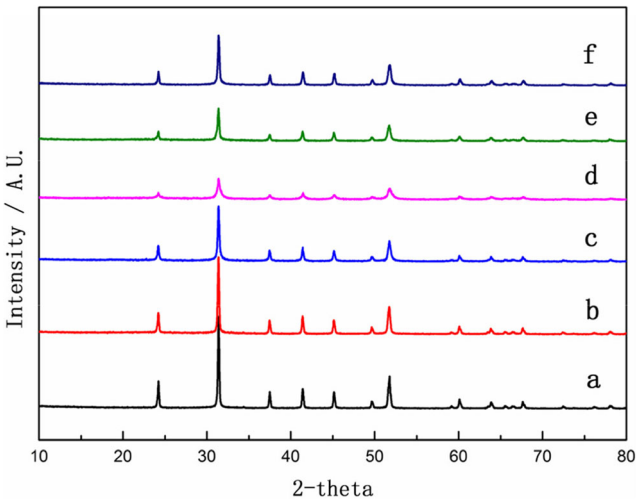

Fig. 4 X-Ray diffraction patterns of $Ni_{0.15}Co_{0.15}Mn_{0.7}CO_3$ collected at different reaction times. **a**–**d** EG-precursors: 2.5 h (**a**), 3 h (**b**), 3.5 h (**c**), aging overnight (**d**). **e**, **f** The pristine: 2.5 h (**e**) and aging overnight (**f**)

Powder X-ray diffraction (XRD) measurements of materials were carried out on a Rigaku 2500 X-ray diffractometer using Cu-Kα radiation. The diffraction data were collected over the range $10° < 2\theta < 80°$. The morphology of the synthesized samples was observed by a JEOL JSM-5600LV scanning electron microscopy (SEM).

The positive electrodes were prepared by mixing 80 wt% prepared powders, 10 wt% carbon conducting additive, and 10 wt% polyvinylidene difluoride (PVDF) binder in *N*-methyl-2pyrrolidone (NMP) solvent. Then, the slurry was cast onto a smooth aluminum foil and then dried. The laboratory half-cell was consisted of a positive electrodes (diameter = 14 mm) and a lithium metal anode separated by a Celgard 2400 polyethylene/polypropylene film and then with the electrolyte of 1 mol/L $LiPF_6$ dissolved in EC/DMC/DEC (1:1:1 by volume). The half-cells were assembled and sealed in an argon-filled glove box and then tested on a LAND-CT2001A battery test system (Jinnuo Wuhan Co. Ltd., P.R. China) in the voltage range of 2.0–4.8 V at room temperature. Electrochemical impedance spectroscopy (EIS) was carried out on an electrochemical workstation (CHI660E, Shanghai Chenhua) in the frequency range from 0.1 MHz to 0.01 Hz.

Results and discussion

The crystals endured two steps during the carbonate precipitation: the formation of crystal nuclei and their growing up which includes each single crystal nucleus development and the agglomeration of some nuclei [17, 24]. The crystallization process could be controlled by a poor solvent [25–27]. In this work, ethylene glycol (EG) is employed to obtain crystals with the desired size and distribution. Figure 2(I) shows the SEM images of the precursors collected in the presence of ethylene glycol (EG precursors) with different reaction time. Primarily, small particles are produced and then combine with each other to form irregular-shaped and micron-sized loose agglomerates (Fig. 2(a) and (a')) before 2.5 h. Thereafter, the particles grow gradually and continue to aggregate (Fig.

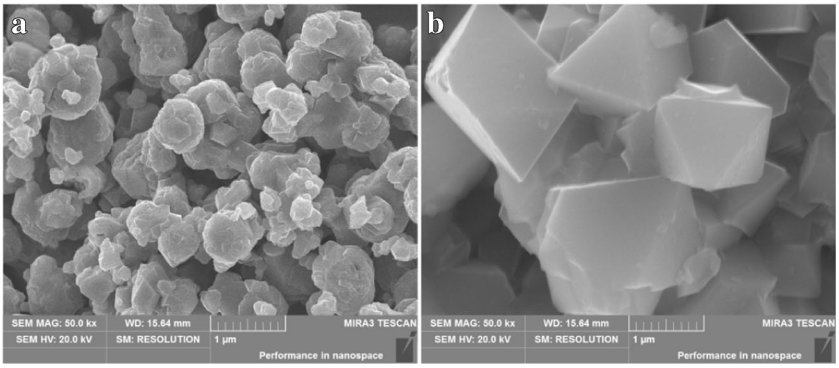

Fig. 5 SEM images of the final powders. **a** EG-assisted sample. **b** The pristine

2(b) and (b')). After 3.5 h, obvious segregation is detected within the agglomerations, and particles continued to grow with a round shape. Finally, the particles obtained after aging overnight are spherical with uniform size. The process of particle growth is shown in schematic illustration (Fig. 3). The precursor particles collected without the addition of ethylene glycol (Fig. 2(II)) are composed of large loose agglomerates with no defined shape. The possible reason is that some extra nucleation sites are available at the surface of the formed particles for further agglomeration without the dispersion of ethylene glycol.

The XRD patterns of precursors with different precipitation time are given in Fig. 4. The diffraction patterns of all samples can be indexed as $MnCO_3$ (JCPDS no. 44-1472) with hexagonal structure ($R\bar{3}$ c space group). The peaks of sample c and d are relatively broad which can be attributed to the small grain size of the precursor particles [28], in agreement with the morphology results. As can be seen from the precursors' XRD results, the phase composition of the precursor does not change as the precipitation reaction proceeds, and the addition of the ethylene glycol in the precursor's process does not affect the formation of the carbonate phase.

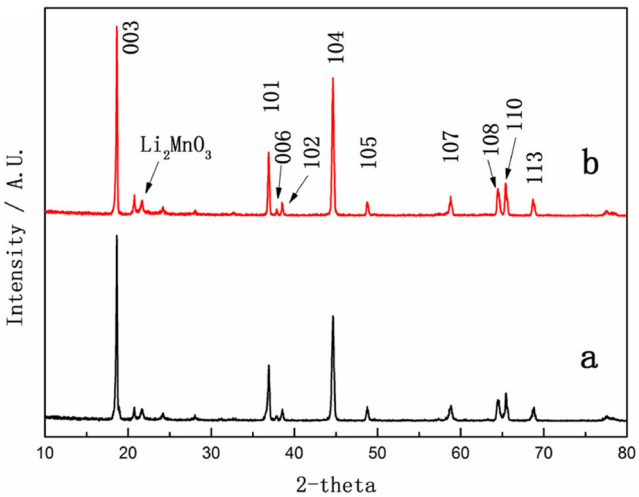

Fig. 6 XRD patterns of the final powders. **a** EG-assisted sample. **b** The pristine

Figure 5 shows the SEM images of the final powders after calcination with Li_2CO_3 at 900 °C. After lithiation, the final $Li_{1.2}Ni_{0.12}Co_{0.12}Mn_{0.56}O_2$ particles retain the morphology of the carbonate precursors even after being recrystallized with lithium sources (Fig. 5). Compared with the particles of the pristine sample (more than 1.5 μm in diameter) (Fig. 5b), the primary particle size of the EG-assisted sample is less than 0.5 μm (Fig. 5a), indicating good electronic ion conductivity. The morphology difference between two samples can be attributed to the usage of novel organic agent (ethylene glycol).

Figure 6 describes the XRD patterns of final powders after calcination with Li_2CO_3 at 900 °C. All main diffraction patterns of the materials can be indexed as hexagonal α-$NaFeO_2$ structure based on the $R\bar{3}$ m space group, except for a broad peak around 21°, which is belonging to the Li_2MnO_3-like (C2/m space group) phase [29–31]. The clear splitting of the (006)/(102) and (108)/(110) peaks in the XRD patterns indicates that the material has a highly ordered layered structure [32]. The lattice parameters of the final materials are calculated by the Rietveld refinements based on the $R\bar{3}$ m space group, and the values are summarized in Table 1. The *c*/*a* ratio of all samples is greater than 4.9, which indicates the formation of layered structure [32]. The intensity ratio (*R*) of $I_{(003)}/I_{(104)}$ is sensitive to the cation distribution in the lattice. It is reported that the undesirable cation mixing would appear when *R* is smaller than 1.2 [33]. In our experiment, all samples have an *R* value higher than 1.2, which means that all samples have a well-ordered hexagonal structure without undesirable cation mixing. The EG-assisted sample exhibits a higher degree value (1.76) than the pristine one (1.37); it reveals that the former has a better layered structure than the latter, which implies that the former might have better electrochemical performance.

Table 1 Lattice parameters of samples

Sample	*a* (Å)	*c* (Å)	*c*/*a*	$I_{(003)}/I_{(104)}$
EG-assisted sample	2.84324	14.20500	4.9961	1.76
The pristine	2.84450	14.20279	4.9931	1.37

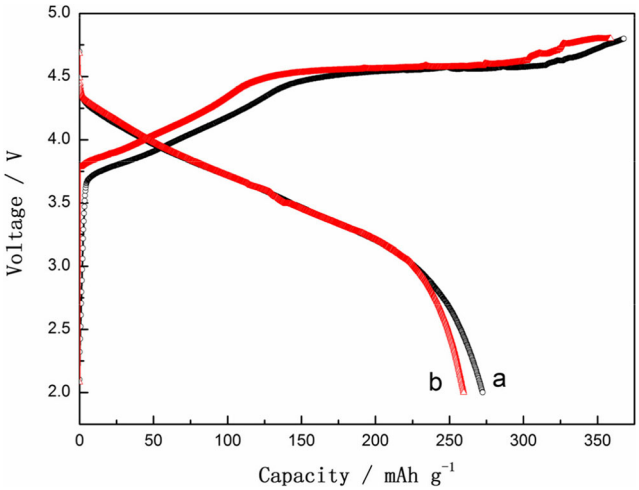

Fig. 7 The first charge-discharge profiles of the Li/$Li_{1.2}Ni_{0.12}Co_{0.12}Mn_{0.56}O_2$ in a CR-2032 lithium cell. **a** EG-assisted sample. **b** The pristine

Figure 7 shows the initial charge-discharge curves of the Li/$Li_{1.2}Ni_{0.12}Co_{0.12}Mn_{0.56}O_2$ at a current density of 12.5 mA g^{-1} (0.05 C). All charge curves are composed of a slope region below 4.5 V and a long plateau at ~4.5 V. The slope region is attributed to the extraction of Li^+ ions from the layered $LiNi_{0.3}Co_{0.3}Mn_{0.4}O_2$ component corresponding to Ni^{2+}/Ni^{4+} and Co^{3+}/Co^{4+} reaction [34]. The long plateau is assigned to the removal of Li_2O from the Li_2MnO_3 structure [34, 35]. This shows the typical electrochemistry characteristic of lithium- and manganese-rich composite material. As shown in Fig. 7, the discharge capacity of the sample prepared without using ethylene glycol (the pristine) is as low as 259.6 mAh g^{-1} when compared with the EG-assisted sample (272.5 mAh g^{-1}). This improved capacity resulted from the addition of ethylene glycol during the carbonate precipitation, which facilitated the formation of small size particles with a uniform size distribution (which was confirmed by the SEM analyses), thereby improving the electrochemical performance.

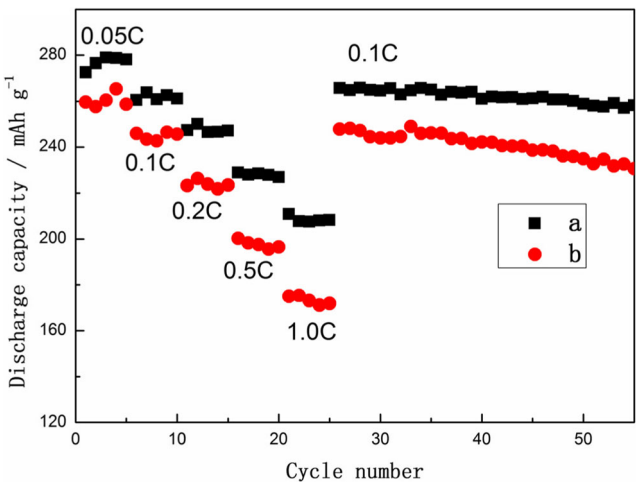

Fig. 8 Rate capabilities of EG-assisted sample (**a**) and the pristine (**b**) at 0.05, 0.1, 0.2, 0.5 and 1.0 C rate

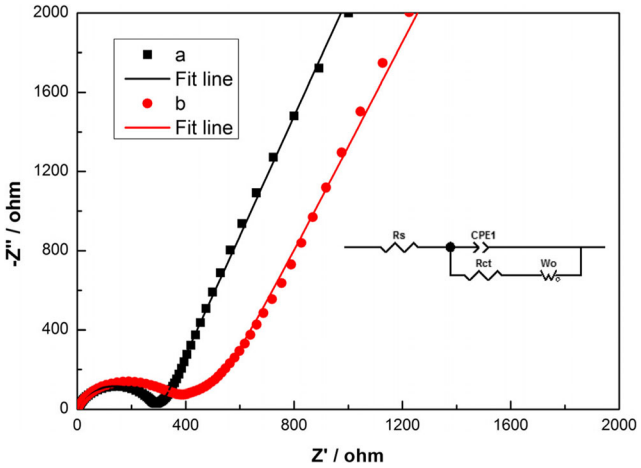

Fig. 9 Nyquist plots of EG-assisted sample (**a**) and the pristine (**b**)

Figure 8 shows the rate capabilities of EG-assisted sample and the pristine from 0.05 to 1 C between 2 and 4.8 V. It can be obviously observed that the EG-assisted sample exhibited higher rate capability than the pristine. These improved rate capability can be attributed to the short Li^+ diffusion path with the small particle size for the EG-assisted sample. When the electrodes are cycled at high rates up to 1.0 C and then recovering back to 0.1 C, the capacities are returned to the initial value, which implied that the high rate cycling (0.2, 0.5, 1.0) did not have any adverse effect on the low rate (0.1 C) capacity. As can be seen, the reversible capacity of the EG-assisted sample is also 258.2 mAh g^{-1} after the 30th charge-discharge cycles with capacity retention of 97.2%, while the pristine one delivered 230.6 mAh g^{-1} with a capacity retention of 93.1% after 30 cycles. Compared to the EG-assisted sample, the large particles of the pristine possibly limited the Li^+ diffusion and led to electrochemically inactivated core, further inflecting the capacity of the material.

In order to comprehensively study the electrochemical properties of the materials, the electrochemical impedance spectroscopies (EIS) of both the EG-assisted sample and the pristine are measured, as shown in Fig. 9. These obtained plots are composed of a semicircle arc and a quasi-straight line, which are assigned to the charge-transfer reaction and the diffusion of Li^+ through the bulk of the material, respectively. These plots are well fitted using the equivalent circuit model (Fig. 9 inset). In the equivalent circuit, R_s and R_{ct} represent the resistance of the solution and charge-transfer resistance in the electrode/electrolyte interface, respectively, CPE indicates the double-layer capacitance, and W_o represents the diffusion-controlled Warburg impedance [36–40]. The EG-assisted sample shows a relatively small charge-transfer resistance (260.4 Ω) by comparison with the value of the pristine (308.4 Ω), which may benefit from the spherical and dispersed morphology.

Conclusion

Mn-based carbonate precursor ($Ni_{0.15}Co_{0.15}Mn_{0.7}CO_3$) is synthesized by the carbonate precipitation in the presence of ethylene glycol. The nucleation and growth of particles are investigated during the carbonate process by monitoring particle morphologies and structures with reaction time. The additive of ethylene glycol shows significant effects on the morphology of the prepared $Ni_{0.15}Co_{0.15}Mn_{0.7}CO_3$ and the electrochemical performance of lithiated $Li_{1.2}Ni_{0.12}Co_{0.12}Mn_{0.56}O_2$. The SEM results show that the particles of the precursors with the presence of ethylene glycol display more spherical and dispersed morphology than those prepared without using ethylene glycol. The final lithiated cathode materials prepared in the presence of ethylene glycol reveal an initial discharging capacity of 272.5 mAh g^{-1} and exhibited about 77.4% capacity retention with regard to the capacity obtained at 0.05 C rate when cycled at 1.0 C rate and more than 97.2% capacity retention after 30 cycles at the 0.1 C rate.

Funding information The work was supported by the National Natural Science Foundation of China (Nos. 51662010, 51364009, 51262008, 51472107, and 51672104), the Educational Commission of Hunan Province, China (Nos. 16B209 and 16B190), the Collaborative Innovation Center of Manganese-Zinc-Vanadium Industrial Technology (the 2011 Plan of Hunan Province), the Research Foundation of Jishou University of Hunan Province, China (Nos. JDLF2016010, 15JDY024, JDSTLY1503, JDZ201503, 201520, and JDST201508), the Aid program (Environment and Energy Materials and Deep Processing of Mineral Resources in Wuling Mountain) for Science and Technology Innovative Research Team in Higher Educational Institutions of Hunan Province (2014[107]), and the Planned Science and Technology Project of Science and Technology Bureau of Xiangxi Tujia and Miao Autonomous Prefecture.

References

1. Tarascon JM, Armand M (2001) Issues and challenges facing rechargeable lithium batteries. Nature 414:359–367
2. Wu X, Xiang Y, Peng Q, Wu X, Li Y, Tang F, Song R, Liu Z, He Z, Wu X (2017) Green-low-cost rechargeable aqueous zinc-ion batteries using hollow porous spinel $ZnMn_2O_4$ as the cathode material. J Mater Chem A 5(34):17990–17997
3. Wang R, Li X, Wang Z, Zhang H (2017) Electrochemical analysis graphite/electrolyte interface in lithium-ion batteries: p-Toluenesulfonyl isocyanate as electrolyte additive. Nano Energy 34:131–140
4. Su M, Wan H, Liu Y, Xiao W, Dou A, Wang Z, Guo H (2018) Multi-layered carbon coated Si-based composite as anode for lithium-ion batteries. Powder Technol 323:294–300
5. Wang J, Liu Z, Yan G, Li H, Peng W, Li X, Song L, Shih K (2016) Improving the electrochemical performance of lithium vanadium fluorophosphate cathode material: focus on interfacial stability. J Power Sources 329:553–557
6. Wu X, Li Y, Xiang Y, Liu Z, He Z, Wu X, Li Y, Xiong L, Li C, Chen J (2016) The electrochemical performance of aqueous rechargeable battery of Zn/$Na_{0.44}MnO_2$ based on hybrid electrolyte. J Power Sources 336:35–39
7. Wang J, Zhang G, Liu Z, Li H, Liu Y, Wang Z, Li X, Shih K, Mai L (2018) $Li_3V(MoO_4)_3$ as a novel electrode material with good lithium storage properties and improved initial coulombic efficiency. Nano Energy 44:272–278
8. Wang R, Wang Z, Li X, Zhang H (2017) Electrochemical analysis the influence of propargyl methanesulfonate as electrolyte additive for spinel LTO interface layer. Electrochim Acta 241:208–219
9. Thackeray MM, Johnson CS, Vaughey JT, Li N, Hackney SA (2005) Advances in manganese-oxide 'composite' electrodes for lithium-ion batteries. J Mater Chem 15(23):2257–2267
10. Wu L, Lu J, Wei G, Wang P, Ding H, Zheng J, Li X, Zhong S (2014) Synthesis and electrochemical properties of xLiMn$_{0.9}$Fe$_{0.1}$PO$_4$·yLi$_3$V$_2$(PO$_4$)$_3$/C composite cathode materials for lithium-ion batteries. Electrochim Acta 146:288–294
11. Liu Y, Zheng S, Wang Q, Fu Y, Wan H, Dou A, Battaglia VS, Su M (2017) Improvement the electrochemical performance of Cr doped layered-spinel composite cathode material $Li_{1.1}Ni_{0.235}Mn_{0.735}Cr_{0.03}O_{2.3}$ with $Li_4Ti_5O_{12}$ coating. Ceram Int 43(12):8800–8808
12. Chen H, He Z, Huang Z, Song L, Shen C, Liu J (2017) The effects of multifunctional coating on Li-rich cathode material with hollow spherical structure for Li-ion battery. Ceram Int 43(12):8616–8624
13. Liu Y, Zhang Z, Fu Y, Wang Q, Pan J, Su M, Battaglia VS (2016) Investigation the electrochemical performance of $Li_{1.2}Ni_{0.2}Mn_{0.6}O_2$ cathode material with $ZnAl_2O_4$ coating for lithium ion batteries. J Alloy Compd 685:523–532
14. Konishi H, Hirano T, Takamatsu D, Gunji A, Feng X, Furutsuki S, Okumura T, Terada S, Tamura K (2018) Mechanisms responsible for two possible electrochemical reactions in $Li_{1.2}Ni_{0.13}Mn_{0.54}Co_{0.13}O_2$ used for lithium ion batteries. J Solid State Chem 258:225–231
15. Ju J-H, Ryu K-S (2011) Synthesis and electrochemical performance of $Li(Ni_{0.8}Co_{0.15}Al_{0.05})_{0.8}(Ni_{0.5}Mn_{0.5})_{0.2}O_2$ with core-shell structure as cathode material for Li-ion batteries. J Alloy Compd 509(30):7985–7992
16. Sun Y-K, Lee B-R, Noh H-J, Wu H, Myung S-T, Amine K (2011) A novel concentration-gradient $Li[Ni_{0.83}Co_{0.07}Mn_{0.10}]O_2$ cathode material for high-energy lithium-ion batteries. J Mater Chem 21(27):10108–10112
17. Wang D, Belharouak I, Koenig GM, Zhou G, Amine K (2011) Growth mechanism of $Ni_{0.3}Mn_{0.7}CO_3$ precursor for high capacity Li-ion battery cathodes. J Mater Chem 21(25):9290–9295
18. Liu J, Chen H, Xie J, Sun Z, Wu N, Wu B (2013) Morphology and particle growth of a two-phase Ni/Mn precursor for high-capacity Li-rich cathode materials. J Appl Electrochem 44(2):225–232
19. Xiang Y, Li J, Wu X, Xiong L, Yin Z (2015) Synthesis and characterization of manganese-rich transition metal carbonate precursor in the presence of ethanol. Adv Powder Technol 26(6):1712–1718
20. Wu F, Wang H, Bai Y, Li Y, Wu C, Chen G, Liu L, Ni Q, Wang X, Zhou J (2017) Hierarchical microspheres and nanoscale particles: effects of morphology on electrochemical performance of $Li_{1.2}Mn_{0.54}Ni_{0.13}Co_{0.13}O_2$ cathode material for lithium-ion batteries. Solid State Ionics 300:149–156
21. Wang M, Luo M, Chen Y, Chen L, Yan S, Ren Y, Chu M (2017) A new approach to improve the electrochemical performance of Li-rich cathode material by precursor pretreatment. J Alloy Compd 696:891–899
22. Zhang J, Guo X, Yao S, Zhu W, Qiu X (2013) Tailored synthesis of $Ni_{0.25}Mn_{0.75}CO_3$ spherical precursors for high capacity Li-rich cathode materials via a urea-based precipitation. J Power Sources 238:245–250
23. Zheng J, Deng S, Shi Z, Xu H, Xu H, Deng Y, Zhang Z, Chen G (2013) The effects of persulfate treatment on the electrochemical properties of $Li[Li_{0.2}Mn_{0.54}Ni_{0.13}Co_{0.13}]O_2$ cathode material. J Power Sources 221:108–113

24. He P, Wang H, Qi L, Osaka T (2006) Electrochemical characteristics of layered $LiNi_{1/3}Co_{1/3}Mn_{1/3}O_2$ and with different synthesis conditions. J Power Sources 160(1):627–632
25. Manoli F, Dalas E (2000) Spontaneous precipitation of calcium carbonate in the presence of ethanol, isopropanol and diethylene glycol. J Cryst Growth 218:359–364
26. Antipov AA, Shchukin D, Fedutik Y, Petrov AI, Sukhorukov GB, Möhwald H (2003) Carbonate microparticles for hollow polyelectrolyte capsules fabrication. Colloid Surf A 224(1–3):175–183
27. Larsen MJ, Thorsen A, Jensen SJ (1985) Ethanol-induced formation of solid calcium phosphates. Calcified Tissue Int 37:189–193
28. Xiang Y, Yin Z, Zhang Y, Li X (2013) Effects of synthesis conditions on the structural and electrochemical properties of the Li-rich material $Li[Li_{0.2}Ni_{0.17}Co_{0.16}Mn_{0.47}]O_2$ via the solid-state method. Electrochim Acta 91:214–218
29. Armstrong AR, Holzapfel M, Novák P, Johnson CS, Kang S-H, Thackeray MM, Bruce PG (2006) Demonstrating oxygen loss and associated structural reorganization in the lithium battery cathode $Li[Ni_{0.2}Li_{0.2}Mn_{0.6}]O_2$. J Am Chem Soc 128(26):8694–8698
30. Rao Penki T, Shanmughasundaram D, Jeyaseelan AV, Subramani AK, Munichandraiah N (2013) Polymer template assisted synthesis of porous $Li_{1.2}Mn_{0.53}Ni_{0.13}Co_{0.13}O_2$ as a high capacity and high rate capability positive electrode material. J Electrochem Soc 161(1):A33–A39
31. Johnson CS, Li N, Lefief C, Thackeray MM (2007) Anomalous capacity and cycling stability of $xLi_2MnO_3{\cdot}(1\text{-}x)LiMO_2$ electrodes (M=Mn, Ni, Co) in lithium batteries at 50°C. Electrochem Commun 9(4):787–795
32. Shi S, Zhang S, Wu Z, Wang T, Zong J, Zhao M, Yang G (2017) Full microwave synthesis of advanced Li-rich manganese based cathode material for lithium ion batteries. J Power Sources 337: 82–91
33. Zhang S, Deng C, Fu BL, Yang SY, Ma L (2010) Synthetic optimization of spherical $Li[Ni_{1/3}Mn_{1/3}Co_{1/3}]O_2$ prepared by a carbonate co-precipitation method. Powder Technol 198(3):373–380
34. Croy JR, Kim D, Balasubramanian M, Gallagher K, Kang S-H, Thackeray MM (2012) Countering the voltage decay in high capacity $xLi_2MnO_3{\bullet}(1\text{-}x)LiMO_2$ electrodes (M=Mn, Ni, Co) for Li^+-ion batteries. J Electrochem Soc 159(6):A781–A790
35. Cabana J, Johnson CS, Yang X-Q, Chung K-Y, Yoon W-S, Kang S-H, Thackeray MM, Grey CP (2011) Structural complexity of layered-spinel composite electrodes for Li-ion batteries. J Mater Res 25(08):1601–1616
36. Zhong S, Hu P, Luo X, Zhang X, Ling W (2016) Preparation of $LiNi_{0.5}Mn_{1.5}O_4$ cathode materials by electrospinning. Ionics 22(11):2037–2044
37. Wang RH, Li XH, Wang ZX, Guo HJ, He ZJ (2015) Electrochemical analysis for enhancing Interface layer of spinel $Li_4Ti_5O_{12}$: p-Toluenesulfonyl isocyanate as electrolyte additive. ACS Appl Mater Interfaces 7(42):23605–23614
38. Xiang Y, Li J, Wu X, Liu Z, Xiong L, He Z, Yin Z (2016) Synthesis and electrochemical characterization of Mg-doped Li-rich Mn-based cathode material. Ceram Int 42(7):8833–8838
39. Zhong S, Wu L, Liu J (2012) Sol-gel synthesis and electrochemical properties of $9LiFePO_4{\cdot}Li_3V_2(PO_4)_3$/C composite cathode material for lithium ion batteries. Electrochim Acta 74:8–15
40. Wu L, Hu Y, Zhang X, Liu J, Zhu X, Zhong S (2018) Synthesis of carbon-coated Na_2MnPO_4F hollow spheres as a potential cathode material for Na-ion batteries. J Power Sources 374:40–47